Journal of Electrical Engineering & Technology (2021) 16:933–939
https://doi.org/10.1007/s42835-021-00661-4

ORIGINAL ARTICLE

Sensorless PMSM Control with Sliding Mode Observer Based on Sigmoid Function

Ningning Ren[1,2] · **Le Fan**[1] · **Zan Zhang**[3]

Received: 9 April 2020 / Revised: 4 November 2020 / Accepted: 7 January 2021 / Published online: 11 February 2021

Abstract
It is impossible to install or apply position sensors appropriately in some special applications of PMSM. Sensorless PMSM control is an appropriate choice to solve some problems in the control of PMSM. It is necessary to acquire an estimated position precisely and avoid the chattering phenomenon for sensorless PMSM control. This paper proposes an algorithm for estimating position with sliding mode observer (SMO) based on sigmoid function, and a sufficient condition that leads SMO into a sliding surface is acquired using Lyapunov stabilization analysis. The outcome of this study shows that SMO based on sigmoid function for sensorless PMSM control can estimate position with high precision and avoid chattering phenomenon under the condition of different velocity and load. However, the estimated position needs to be compensated for according to load, and the compensating value is in proportion to the value of the current.

Keywords PMSM · Sigmoid · Sliding mode observer (SMO)

1 Introduction

With the development of permanent magnet materials, permanent magnet synchronous motor (PMSM) has the advantages of no rotor loss, high power density, energy efficiency, and good static performance [1–4]. It has attracted widespread attention and recognition. In general, PMSM needs to be controlled to get constant torque according to the position of the rotor. While the encoder and the rotary transformer have been used to detect the position of the rotor, it increases costs, mechanical instabilities, and the complexity of the system. Meanwhile, the position sensor is sensitive to temperature and vibration, which makes it impossible to install and apply in some special applications [5]. Therefore, sensorless control is gaining increasing attention. Sensorless technology has always been a hot topic, including rotor position information derived through the direct detection of voltage and current [6], linear observer [7], model reference adaptive control methods [8], and nonlinear estimation based on the extended Kalman filter algorithm [9, 10]. However, these technologies have some shortcomings, such as DC offset, non-global convergence, parameter dependence, and large amounts of computing.

Because of the advantages of fast dynamic response, insensitivity to parameter variations, and strong robustness [11, 12], sliding mode observer (SMO) is widely used for the sensorless control of PMSM [13, 14]. Sensorless control based on SMO is an appropriate method to estimate the position according to electromotive force (EMF). In the stator voltage equation, the EMF is processed as a disturbance, and any interference is considered to be a part of EMF. Chattering problem, caused by the discontinuous switch character of sliding mode variable structure control methods, is the main obstacle in using SMOs as back EMF observers [11].

Several methods have been proposed for reducing the effect of chattering on position estimation in SMO. In [15], an iterative sliding mode observer (ISMO) is proposed for the robust sensorless control of a PMSM with

This work was supported in part by the Key Research of Development and Promotion of Henan Province under Grant 212102210250, and in part by the Key Research of Development and Promotion of Henan Province under Grant 202102210307.

✉ Ningning Ren
renning66@163.com

[1] Henan Polytechnic Institute, NanYang 473000, Henan Province, China

[2] Nanyang Explosion Protected Electrical Apparatus Research Institute, NanYang 473000, Henan Province, China

[3] Xuchang University, XuChangHenan Province 461000, China

variable parameters. The proposed ISMO improves the performance of the sensorless technique by iteratively applying the observer 4 times in a current regular period, which reduces the error of back EMF estimation. However, the ISMO requires more running time than conventional SMO. In [16], the chattering noise is reduced by introducing the fuzzy control algorithm to effectively adjust the switching gains according to the sliding mode arrival condition. However, the addition of fuzzy control increases the complexity of the algorithm.

The method based on switching function is another main method to reduce the effect of chattering on position estimation. The sign function is used to enter into the sliding surface of the conventional SMO. However, the step sign function demanding higher requirements of the low-pass filtering may cause the buffeting phenomenon, resulting in large delay, reducing the accuracy of position estimation. To reduce the chattering problem, a sigmoid function is proposed to replace the sign function. In [17], a sigmoid function with variable boundary layers is used as the switching function. The width of the boundary layers must be adjusted according to velocity, otherwise chattering or steady-state error will occur.

In this paper, sensorless PMSM control with SMO based on sigmoid function is presented. First, the SMO model is derived based on the sigmoid function in this paper according to the mathematical model of the IPMSM. Second, sliding mode gain k and sufficient condition under which SMO can enter into the sliding surface are obtained using Lyapunov stability analysis method. The key parameter a in the sigmoid function is discussed. Finally, the results of the simulation and experiment show that the sigmoid function can eliminate the chattering phenomenon, and the accuracy of the estimated position is guaranteed.

2 Sliding Mode Observer Model of IPMSM Based on Sigmoid Function

Considering the salient effect, the relationship of PMSM is shown below in the coordinate system $A-B-C$,$\alpha-\beta$,$d-q$.

The voltage equation in the coordinate system $d-q$ is:

$$\begin{bmatrix} u_d \\ u_q \end{bmatrix} = \begin{bmatrix} R+pL_d & -\omega L_q \\ \omega L_d & R+pL_q \end{bmatrix} \begin{bmatrix} i_d \\ i_q \end{bmatrix} + \begin{bmatrix} 0 \\ \omega\psi_f \end{bmatrix} \tag{1}$$

Because the first matrix of the right part of the Eq. (1) is asymmetric, this matrix can be transformed to be of odd symmetry.

$$\begin{bmatrix} u_d \\ u_q \end{bmatrix} = \begin{bmatrix} R+pL_d & -\omega L_q \\ \omega L_q & R+pL_d \end{bmatrix} \begin{bmatrix} i_d \\ i_q \end{bmatrix} + \begin{bmatrix} 0 & 0 \\ \omega(L_d-L_q) & -pL_d-L_q \end{bmatrix} \begin{bmatrix} i_d \\ i_q \end{bmatrix} + \begin{bmatrix} 0 \\ \omega\psi_f \end{bmatrix} \tag{2}$$

According to the coordinate transformation, Eq. (2) is transformed under the coordinate $\alpha-\beta$ system.

$$\begin{bmatrix} u_\alpha \\ u_\beta \end{bmatrix} = \begin{bmatrix} R+pL_d & -\omega(L_d-L_q) \\ \omega(L_d-L_q) & R+pL_d \end{bmatrix} \begin{bmatrix} i_\alpha \\ i_q \end{bmatrix} + \left\{ (L_d-L_q)\left(\omega i_d - \dot{i}_q\right) + \omega\psi_f \right\} \begin{bmatrix} -\sin\theta \\ \cos\theta \end{bmatrix} \tag{3}$$

The second term of (3) is the extension EMF (EEMF).

$$\begin{cases} ee_\alpha = -\sin\theta\left((L_d-L_q)\left(\omega i_d - \dot{i}_q\right) + \omega\psi_f \right) \\ ee_\beta = \cos\theta\left((L_d-L_q)\left(\omega i_d - \dot{i}_q\right) + \omega\psi_f \right) \end{cases} \tag{4}$$

So, the position of rotor is

$$\theta = \tan^{-1}\left(-\frac{ee_\alpha}{ee_\beta}\right) \tag{5}$$

Equation (3) can be written in the form of state equation.

$$\begin{bmatrix} \dot{i}_\alpha \\ \dot{i}_\beta \end{bmatrix} = \begin{bmatrix} -\frac{R}{L_d} & -\omega\frac{L_d-L_q}{L_d} \\ \omega\frac{L_d-L_q}{L_d} & -\frac{R}{L_d} \end{bmatrix} \begin{bmatrix} i_\alpha \\ i_\beta \end{bmatrix} - \frac{1}{L_d}\begin{bmatrix} ee_\alpha \\ ee_\beta \end{bmatrix} + \frac{1}{L_d}\begin{bmatrix} u_\alpha \\ u_\beta \end{bmatrix} \tag{6}$$

From the equation, we can observe that the EEMF includes significant information. The position of the rotor can be obtained through the estimated EEMF.

When resistance deviation is considered, based on the method of state observer and Eq. (6), SMO model of EEMF is

$$\begin{bmatrix} \dot{\hat{i}}_\alpha \\ \dot{\hat{i}}_\beta \end{bmatrix} = A\begin{bmatrix} \hat{i}_\alpha \\ \hat{i}_\beta \end{bmatrix} + B\left(\begin{bmatrix} \hat{u}_\alpha \\ \hat{u}_\beta \end{bmatrix} - k\begin{bmatrix} H(\bar{i}_\alpha) \\ H(\bar{i}_\beta) \end{bmatrix} \right) \tag{7}$$

$$A = \begin{bmatrix} -\frac{R}{L_d} & -\omega\frac{L_d-L_q}{L_d} \\ \omega\frac{L_d-L_q}{L_d} & -\frac{R}{L_d} \end{bmatrix}, B = \begin{bmatrix} \frac{1}{L_d} & 0 \\ 0 & \frac{1}{L_d} \end{bmatrix},$$

$\bar{i}_\alpha = \hat{i}_\alpha - i_\alpha$, $\bar{i}_\beta = \hat{i}_\beta - i_\beta$

$\hat{i}_\alpha$, $\hat{i}_\beta$—the estimated current.

$\bar{i}_\alpha$, $\bar{i}_\beta$—the error of the estimated current.

Equation (7) is the sliding mode state observer. When the error of the estimated current is processed with sign function in the traditional SMO, the estimated EMF is a modulation waveform, and the cutoff frequency of the low pass filter is designed to be very low. This causes the estimated position lag, while the estimated position has jitter problems. The performance of the whole system comes down or does not function properly (Fig. 1). Therefore, the sigmoid function is applied to the SMO in this study.

The expression of the sigmoid function is

$$\begin{bmatrix} H(\bar{i}_\alpha) \\ H(\bar{i}_\beta) \end{bmatrix} = \begin{bmatrix} \left(\frac{2}{1+\exp(-a\cdot\bar{i}_\alpha)}\right) - 1 \\ \left(\frac{2}{1+\exp(-a\cdot\bar{i}_\beta)}\right) - 1 \end{bmatrix} \tag{8}$$

In Eq. (8), a is a constant used for adjusting the slope of the sigmoid function, and when a is close to infinity, the sigmoid function is transformed into a sign function.

According to (6) and (7), the estimated EEMF is

$$\begin{cases} \hat{ee}_\alpha \approx k \cdot H(\bar{i}_\alpha) \\ \hat{ee}_\beta \approx k \cdot H(\bar{i}_\beta) \end{cases} \tag{9}$$

The diagram of the estimated position can be obtained from the analysis above, as shown in Fig. 2.

The diagram of SMO based on the sigmoid function for sensorless PMSM control is shown in Fig. 3. Phase voltage is calculated based on the voltage of the DC bus and SVPWM switching state. The measured phase currents are transformed into i_α, i_β, then i_α, i_β are placed into the SMO model with phase voltage, and the position is obtained according to (5) and (9).

3 The stability Analysis of the System

The key of SMO for PMSM is to ensure that the estimated values can converge to the sliding surface. When the current error is negative, its differential value is positive; when the current error is positive, its differential value is negative. This law is presented by the non-negative Lyapunov function in Eq. (10).

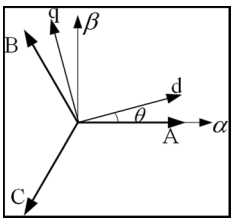

Fig. 1 Relationship among three references

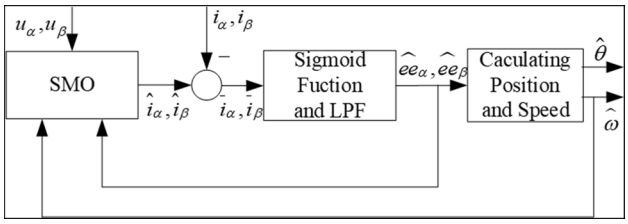

Fig. 2 SMO based on sigmoid function

$$V = \frac{1}{2}s^T s \tag{10}$$

$s = [\,\bar{i}_\alpha \;\; \bar{i}_\beta\,]^T$ is estimated current error.

According to the Lyapunov stability theory, the derivative of V must be less than zero to ensure that the stable point has asymptotic stability. The derivative of the Eq. (11) is

$$\dot{V} = \bar{i}_\alpha \cdot \dot{\bar{i}}_\alpha + \bar{i}_\beta \cdot \dot{\bar{i}}_\beta < 0 \tag{11}$$

Substituting (6) and (7) into (11), Eq. (12) is obtained.

$$\begin{aligned} V = &-\frac{R}{L_d}\left(\bar{i}_\alpha^2 + \bar{i}_\beta^2\right) \\ &+\frac{1}{L_d}\left[\bar{i}_\alpha\left(ee_\alpha - kH(\bar{i}_\alpha)\right) + \bar{i}_\beta\left(ee_\alpha - kH(\bar{i}_\beta)\right)\right] \end{aligned} \tag{12}$$

According to (8), $H(\bar{i}_\alpha)$ and $H(\bar{i}_\beta)$ are increasing functions, which pass through the origin and are restricted within ±1. Therefore, a sufficient condition to Eq. (12) is (13).

$$k \geq \max\left(\left|ee_\alpha\right|, \left|ee_\beta\right|\right) \tag{13}$$

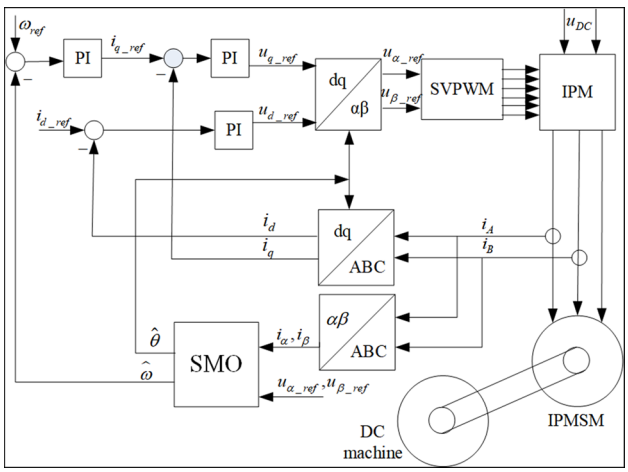

Fig. 3 Diagram of PMSM sensorless control with SMO based on sigmoid function

Table 1 The parameters of PMSM

Pair of poles	1
Rated speed	1200 rpm
Stator resistance	2.93Ω
d-axis inductance	10.5 mH
q-axis inductance	22.1 mH
rated current	5 A
rated power	3.3 kw

Equation (13) determines the feedback coefficient of SMO to guarantee that SMO based on the sigmoid function will converge to the sliding surface. At the same time, k determines the speed of convergence. At the switching point of sliding mode, the change of the current error will lead to the change of the sigmoid function; motor voltage equation is equivalent to a first-order incentive system, and the main reason of the jitter is the response of the stimulus in SMO. The higher the number of k, the greater the response value. Therefore, the jitter and stability must reach an equilibrium point with the selection of k. Furthermore, a must also be selected appropriately; if a is too small, it will affect the stability of the system or the speed of convergence; if a is too large, the jitter problem will appear. Under the condition of proper a and k, the sigmoid function, instead of sign function, has a significant advantage in the jitter problem.

4 The Simulation and Experimental Results

The parameters of the motor are shown in Table 1. The motor was connected to the DC generator with a belt as the load. Selecting the photoelectric encoder of Autonics, the position can be used as the actual position. $a = 1$ in the sigmoid function, the gain of current error is $K = 250$.

In this study, the current waveforms are obtained by the current sensor. The actual position θ, estimate position $\widehat{\theta}$, and estimation error $\theta - \widehat{\theta}$ are obtained by the TLC7528 after processed by a DSP. There are only two DA channels in TLC7528, so the three waveforms about the position cannot appear in the oscilloscope at the same time. The experiments were run under the conditions of sensorless PMSM control (Fig. 4).

The calculated electromotive force is shown in Fig. 5a. The upper part in the figure is the waveform before the low-pass filter, and the lower part is the waveform after the low pass filter. There is no high-frequency component, and there is little delay in the lower part of Fig. 5a. The spectrum analysis of the waveform before the low-pass filter is shown

Fig. 4 The experimental platform

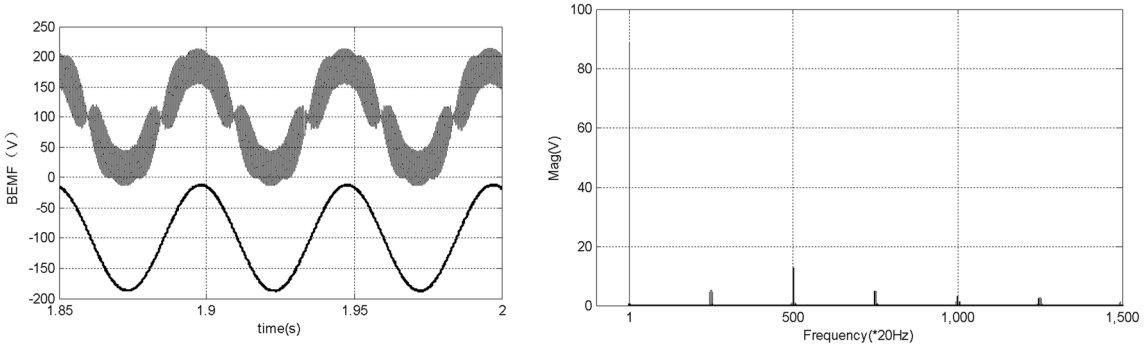

(a) The estimated EEMF **(b)** Frequency of estimated EEMF

Fig. 5 Estimated EEMF and its frequency

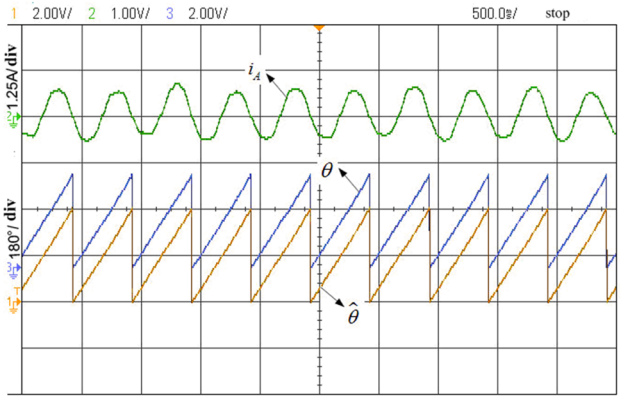

(a) A-phase current, actual position, and estimated position

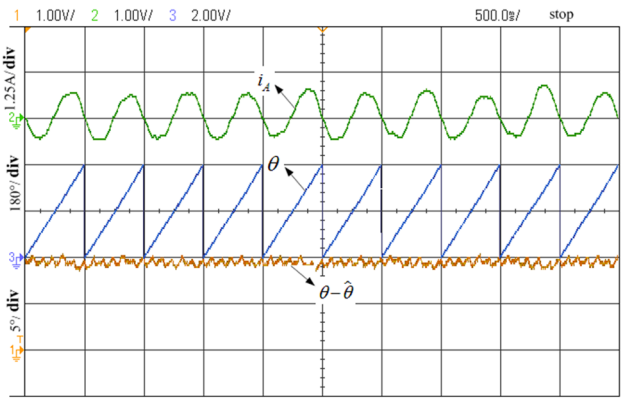

(b) A-phase current, actual position, and estimated error

Fig. 6 Position estimating at 2 Hz and no load

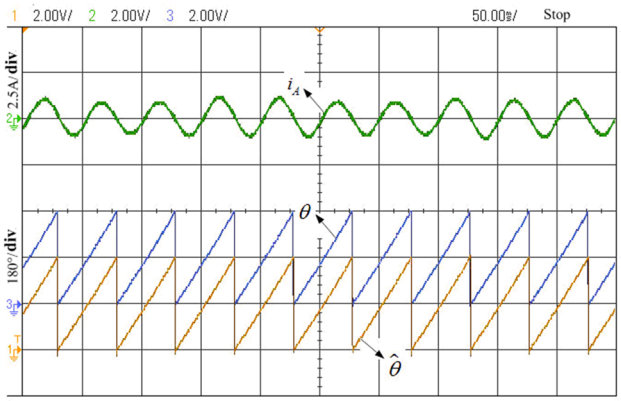

(a) A-phase current, actual position, and estimated position

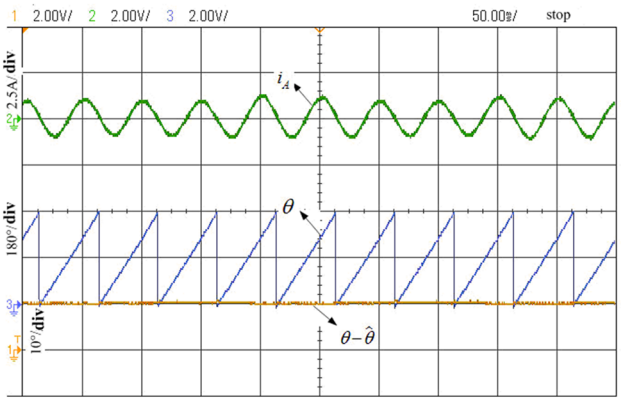

(b) A-phase current, actual position, and estimated error

Fig. 7 Position estimating at 20 Hz and no load

in Fig. 5b. The frequency of harmonics is $250 * n$ times of the fundamental. The fundamental component is the electrical frequency of the machine, which is far lower than the frequency of harmonics. Therefore, jitter and delay are produced substantially.

While there is no load at 2 Hz, the current of phase A, actual position, and estimated position are shown in Fig. 6a. The A-phase current, actual position, and estimated error are shown in Fig. 6b. The actual position coincides with the estimated position, and the estimated error is significantly small. This algorithm is well verified in low-speed operating conditions.

While there is no load at 20 Hz, the position and current are shown in Fig. 7. Compared with 2 Hz, there are higher estimation accuracy and better matching degree.

The position estimation at 20 Hz and sudden load are shown in Fig. 8. When loading suddenly, the estimated error increases from 0º to 5º.

The figure of stable operation is shown in Fig. 9 at 20 Hz and loading; when loaded stable operation, the position error is stable ahead of the actual position about 5º. The error can be compensated for according to the load and is easy to implement; a similar phenomenon also appears in [18]. The stable estimated error in the figure shows that there is no chattering phenomenon.

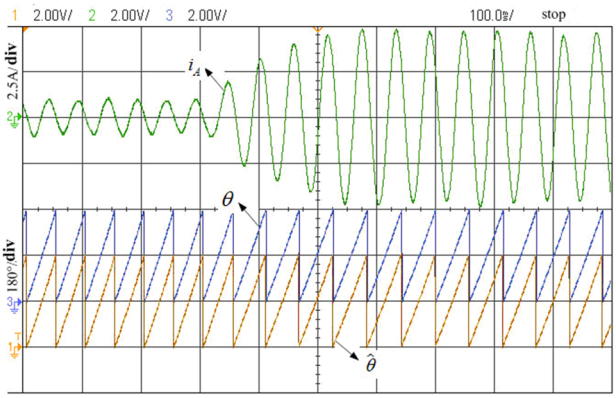

(a) A-phase current, actual position and estimated position

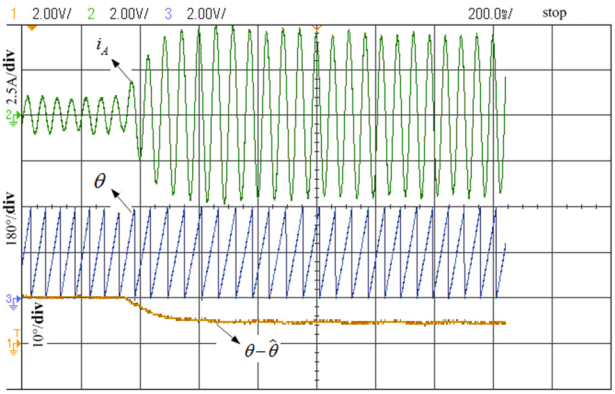

(b) A-phase current, actual position, and estimated error

Fig. 8 Position estimating at 20 Hz and sudden load

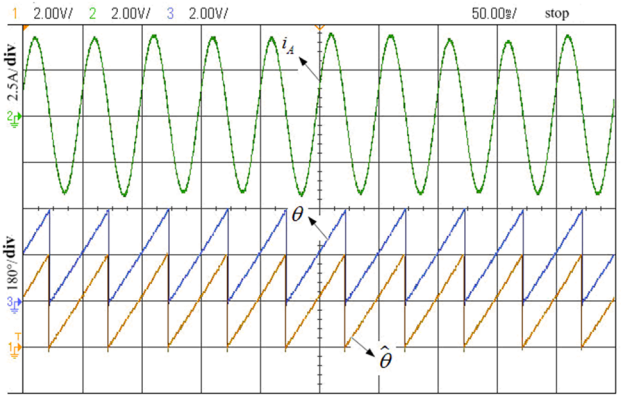

(a) A-phase current, actual position, and estimated position

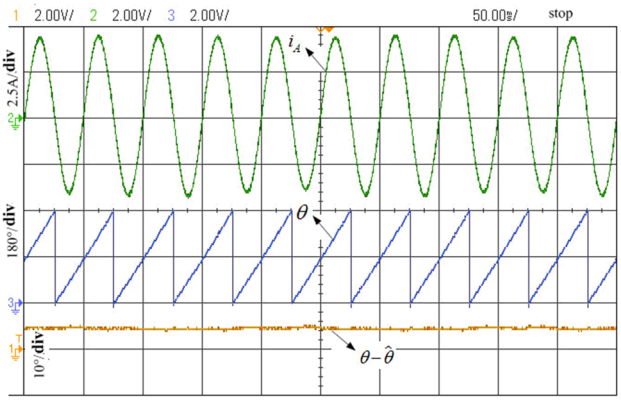

(b) A-phase current, actual position, and estimated error

Fig. 9 Position estimating at 20 Hz and full load

5 Conclusion

The SMO of the sigmoid function is based on BEMF of the IPMSM. The obtained findings of this study are:

1. Lyapunov stability analysis was used to obtain the sliding mode gain range
2. 2. The sigmoid function to eliminate the chattering phenomenon of SMO is analyzed.
3. 3. The experimental results show that this method can suppress and eliminate the buffeting phenomenon and proved that the SMO of the sigmoid function has much higher accuracy.
4. 4. The estimated position which is ahead of the actual position on load needs further analysis to reduce or eliminate.

References

1. Zhou Yu, Li H, Wang W, Cao Q, Zhou S (2015) Improved method for calculating magnetic field of surface-mounted permanent magnet machines accounting for slots and eccentric magnet pole. J Electr Eng Technol 10(3):1025–1034
2. Chen Z, Tomita M, Doki S, Okuma S (2003) An extended electromotive force model for sensorless control of interior permanent magnet synchronous motors. IEEE Trans Indus Electron 50(2):288–295
3. Zhou Y, Li HS, Meng GW, Zhou S, Cao Q (2015) Analytical calculation of magnetic field and cogging torque in surface-mounted permanent-magnet machines accounting for any eccentric rotor shape. IEEE Trans Industr Electron 62(6):1–1
4. M. Aryanezhad A novel designing approach to dual rotor switched reluctance motor based electric vehicles. In: 2015 30th International Power System Conference (PSC); IEEE published, 2015:54-59
5. Maidum M (1992) Rotor position estimation scheme of a permanent magnet synchronous machine for high performance variable speed drive. Houston, USA, IEEE IAS, pp 48–53
6. Bose Bimal K (2003) Modern power electrics and AC drives. China Machine Press, Beijing, pp 157–160
7. YS Kim, SK Kim, MRAS based sensorless control of permanent magnet synchronous motor. In: IEEE SICE Annual Conference, 2003, Fukui, Japan:1632–1637.
8. Zhe S, Rong-xiang Z, Ru-zhen D (2007) Research on sensorless control method of PMSM based on an adaptive sliding mode observer. Proc CSEE 27(3):23–27
9. Mercorelli P (2012) A hysteresis hybrid extended kalman filter as an observer for sensorless valve control in camless internal combustion engines. IEEE Trans Ind Appl 48(6):1940–1949
10. Mercorelli P (2012) A two-stage augmented extended kalman filter as an observer for sensorless valve control in camless internal combustion engines. IEEE Trans Industr Electron 59(11):4236–4247
11. Wang Y, Yongxiang Xu, Zou J (2019) Sliding mode sensorless control of PMSM with inverter nonlinearity compensation. IEEE Trans Power Electron 34(10):10206–10220
12. Liang D, Li J, Ronghai Qu, Kong W (2018) Adaptive second-order sliding-mode observer for PMSM sensorless control considering VSI nonlinearity. IEEE Trans Power Electron 33(10):8994–9004
13. Wen-qi LU, Yu-wen HU, Du X (2010) Sensorless vector control using a novel sliding mode observer for PMSM speed control system. Proc CSEE 30(33):78–83
14. Ran L, Zhao G, Xu S (2012) Sensorless control of permanent magnet synchronous motor based on extended sliding mode observer. Trans China Electrotech Soc 27(3):79–85
15. Lee H, Lee J (2013) Design of iterative sliding mode observer for sensorless PMSM control. IEEE Trans Control Syst Technol 21(4):1394–1399
16. Sheng L, Li W, Wang Y, Fan M, Yang X (2017) Sensorless control of a shearer short-range cutting interior permanent magnet synchronous motor based on a new sliding mode observer. IEEE Access 5:18439–18450
17. Kim H, Son J, Lee J (2011) A high-speed sliding-mode observer for the sensorless speed control of a pmsm. IEEE Trans Indus Electron 58(9):4069–4077
18. Corley MJ, Lorenz RD (1998) Rotor position and velocity estimation for a salient-pole permanent magnet synchronous machine at standstill and high speeds. IEEE Trans Indus Appl 34(4):784–789

Nningning Ren received the M.S degree in control theory and control engineering from the College of Electrical Engineering and Automation, Henan Polytechnic University, Jiaozuo, China, in 2011 and the Ph.D degree in Electrical Engineering from the College of Electrical Engineering, Naval University of Engineering, Wuhan, China, in 2018. He is currently a Lecturer with the College of mechanical and electrical automation, Henan Polytechnic Institute. His current research interests include power electronic and design and control of permanent-magnet machines. Since 2020, he has been working of Postdoctoral research at the Nanyang Explosion Protected Electrical Apparatus Research Institute, China.

Le Fan received the M.S degree in control theory and control engineering from School of Electrical Engineering and Automation, Henan Polytechnic University, Jiaozuo, China, in 2011. She is currently a Lecturer with the College of mechanical and electrical automation, Henan Polytechnic Institute. Her current research interests include power electronic and design and control of permanent-magnet machines.

Zan Zhang received the M.S degree in Electric Machines and Electric Apparatus from the College of Electrical Engineering and Automation, Henan Polytechnic University, Jiaozuo, China, in 2012 and the Ph.D degree in Electrical Engineering from the School of Automation, Northwestern Polytechnical University, Xian, China, in 2018. He is currently a Lecturer with the School of Electrical and Mechanical Engineering, Xuchang University. His current research interests include power electronic and design and control of permanent-magnet machines.